Scientia Iranica A (2023) 30(3), 918–935

Sharif University of Technology
Scientia Iranica
Transactions A: Civil Engineering
http://scientiairanica.sharif.edu

Experimental study on performance of repaired and strengthened unreinforced masonry walls using polypropylene bands

S. Ebrahimzadeh and K. Nasrollahzadeh*

Department of Civil Engineering, K. N. Toosi University of Technology, Tehran, P.O. Box 15875-4416, Iran.

Received 25 November 2021; received in revised form 25 March 2022; accepted 29 August 2022

KEYWORDS
Unreinforced masonry wall;
Damaged URM wall;
Repair and strengthening;
Experimental study;
Quasi-static lateral loading;
Polypropylene (PP) band;
Strengthening materials.

Abstract. This paper proposes a strengthening method for improving the seismic performance of Unreinforced Masonry (URM) brick walls. What is noteworthy regarding the proposed technique is the low price and easy application of polypropylene (PP) bands, which are widely used in the packaging industry. Three half-scale specimens were tested under cyclic lateral loading simultaneously upon imposing a constant vertical load. First, the URM wall was tested up to a certain drift in which a reduction in lateral capacity was recorded. According to the crack pattern observed on the wall surface, a repair strategy was taken to upgrade the damaged wall in the shortest possible time and with minimum manpower. In doing so, horizontal PP bands were employed to wrap the wall. The repair technique stopped the spread of cracks and prevented reduction in lateral capacity. Besides, the third specimen, which is identical to the URM wall but is strengthened by PP bands, was tested and it developed a superior performance by changing the failure mode and increasing the maximum strength, the strength at maximum displacement, and maximum displacement by 88%, 38%, and 185%, respectively, compared to URM wall.

1. Introduction

Conventional methods used to reinforce masonry specimens to increase the bearing capacity and improve the performance of the structure include coating of the walls with a layer of mortar [1] or simultaneous use of cement mortar with metal mesh or steel mesh [2]. Specifically, in this method, the surfaces of the tested specimens are reinforced with a layer of steel mesh and cement-sand mortar with a thickness of 30 to 100 mm [3]. One of the most popular polymer fibers used to increase the strength and ductility of masonry specimens of the studies is called Fiber Reinforced Polymers or FRP [4]. Regarding retrofitting methods that use polymer fibers and cement-sand mortar simultaneously, several techniques such as Textile Reinforced Concrete (TRC) [5], Fabric Reinforced Cementitious Matrix (FRCM) [6,7], and Engineered Cementitious Composite (ECC) [8,9] can be mentioned. By using the unreinforced cement mortar, traditional retrofitting methods improve the tensile strain capacity of the tested specimens by less than 0.015% and increase the bearing capacity of the specimens by a maximum of 3.5 MPa. The primary advantages of using polymer fibers include the ease of execution, no increase in the weight of the structure [10], and improvement of the energy dissipation of masonry walls [11]. Despite the mentioned advantages, the use of FRP in strengthening and retrofit is subject to such drawbacks as inability

*. *Corresponding author. Tel.: +98 21 88779473; Fax: +98 21 88779476*
E-mail address: nasrollahzadeh@kntu.ac.ir (K. Nasrollahzadeh)

doi: 10.24200/sci.2022.59449.6252

to be used on wet surfaces, reduced performance at high temperatures and in alkaline environments (which are an integral part of masonry structures), inevitable potential hazards for workers, and the incompatibility of resin with the masonry materials. However, the use of FRCM, TRM, and FRM methods has resolved the mentioned shortcomings. Hence, benefits such as reversibility (separation without damage to the structural layers) and no conflict with the architecture of the structure (due to the low thickness of the coat on the wall) are brought to the retrofitting system and the seismic performance improvement of the structure. Polypropylene (PP) bands represent another example of polymer fibers used to reinforce masonry walls [12]. The advantage of using these bands over other retrofitting techniques is the easy access and low price of these fibers. Cost-effectiveness of the retrofitting materials such as PP mesh and metal mesh as well as the significant impact on increasing shear strength, improving ductility, and the energy dissipation capacity of different types of masonry structures have led to the widespread use of these materials by researchers such as Nayak et al. [13] and Heydariha et al. [14]. Both reinforcement methods are effective in preventing a sudden collapse of the masonry wall resulting from poor ductility and brittle behavior of the materials. Banerjee et al. [15] tested 32 full- and half-scale specimens under diagonal compression loading to improve the strength of the wallets reinforced with PP bands and metal mesh. The improved performance of PP band-reinforced structures results from the fact that the PP band causes the integrity of the structures and contributes to the stress distribution. Meguro et al. [16] conducted shaking table tests on the 1:4-scale models including Unreinforced Masonry (URM) and PP mesh-reinforced models, and the results suggest the improved energy dissipation capacity and increased deformation capacity. Furthermore, with the aim of comparing key parameters such as seismic performance, easy application, and cost-effectiveness, Nissanka et al. [17] compared the steel mesh and PP mesh materials retrofitting techniques. Macabuag et al. [18] investigated the effect of the PP bands directions on the grids use to improve the shear strength of masonry walls. The results indicate that the vertical bands stretch when slipping occurs, hence preventing slipping. The horizontal bands increase the friction of the bricks in each row placed on one another. The present research addresses the rapid retrofitting and repair method for the damaged masonry wall as well as retrofitting of Unreinforced Masonry Walls (URMW) with the least amount of PP and cement-sand mortar. The bands are used to repair the damaged specimen in order to prevent the reduction of bearing capacity and the spread of the crack pattern. Also, to strengthen the masonry wall, the combination of PP band and the least amount of cement-sand mortar increases the bearing capacity, causes lateral displacement, and changes the failure mode.

2. Experimental program

2.1. Characteristics of the materials

2.1.1. Mortar and masonry tests

The cement-sand mortar with a volume ratio of 1:6 (cement:sand) and a thickness of 12 mm was used evenly in all rows to construct the wall. According to [19], mortar composed of Portland cement and river bed sand at a ratio of 1:6 has weak shear strength and is considered as the lower bound of the shear strength of existing masonry buildings in Iran. It is noted that the mortar used herein is the combination of cement and sand, whereas other types of mortar (e.g., lime-based one) are reported in the literature. In the present study, proper workability of mortar as well as the common practice in Iranian masonry construction are the basis for choosing 1:3 for water/cement ratio. In order to determine the compressive strength of the mortar used in the construction of masonry walls, according to the standard [20], 12 cubic mortar prisms with approximate dimensions of $50 \times 50 \times 50$ mm were made. After 28-day curing of mortar specimens using a wet jute canvas, by applying uniaxial stress to the specimens, parameters such as compressive strength of mortar were determined. Moreover, the shear strength of the mortar of the building materials in the in-situ shear test of the mortar was tested according to the standard [21] and Ref. [22] in the outer row of the wall. The test was done experimentally by moving a brick based on the adjacent bricks. To conduct the in-situ shear strength test, the brick wall and mortar around it were emptied from three different heights, and a sheet with the dimensions of the hydraulic jackshaft chamber was placed to apply uniform stress to the entire surface of the brick specimen in front of the hydraulic jack. According to Eq. (1), the effect of stress resulting from the in-situ gravity load of the test specimen should be subtracted from it. The equation presented to calculate the shear strength of the mortar is as follows:

$$v_{to} = \frac{V_{test}}{A_b} - P_{D+L}, \tag{1}$$

$$v_{me} = \frac{0.75(0.75 \times V_{to} + \frac{P_D}{A_n})}{1.5}. \tag{2}$$

In Eqs. (1) and (2), V_{test} is the force obtained from the in-situ shear test, v_{to} the average shear stress, A_b the surface of the upper and lower horizontal mortar, A_n the net area of mortar, P_D the vertical dead load up to the mortar level of the location of the sample, and v_{me} is the shear stress measured by

the in-situ test. It should be noted that the mortar shear strength value obtained from the in-situ shear test was calculatedin the range between 0.11 and 0.2 MPa, in which, assuming the same thickness of the horizontal mortar, the average strength of 0.15 MPa was calculated. The value obtained from the uniaxial pressure test on the fabricated specimens inhibited in the test setup using a multilayer sheet on both sides was equal to the mean of 0.09 MPa. Table 1 shows the specifications of the cement-sand mortar.

2.1.2. Clay brick

The brick used to make the specimens (solid clay brick) is proportional to a half-scale masonry wall of dimensions of 96 × 50 × 36 mm (length × width × height) and a specific mass of 1943 kg/m^3. All tests were done to determine the mechanical properties of the brick in accordance with standards [23]. The compressive strength of the bricks used in this experimental program is determined by applying a uniaxial pressure test to 9 specimens. In order to determine the water absorption of the specimens according to the method presented in [24], the bricks are first completely submerged for 24 hours, and to determine the water absorption, the weights of the specimens are recorded before and after drying at room temperature. Moreover, according to standard [25], six masonry prisms consisting of five rows of single bricks were constructed and tested under uni-axial compression to determine the compressive strength of masonry units (i.e., the assemblage of bricks and mortar). Table 2 shows the mechanical properties of bricks, such as mean compressive strength, modulus of elasticity, flexural strength, and coefficient of variation. In addition, it reports the mean compressive strength of the masonry units.

2.1.3. PP bands

To calculate the tensile strength, the bands were stretched in two ways. In the first case, the PP bands were subjected to uniaxial tension using Universal Machine. In the second case, the PP bands connected by a metal clamp in the middle were stretched. It should be mentioned that two bands are cut to equal length, and each of them passes through the metal clamp with equal overlap and is punched together by special punching pliers at a point where the clamp is located. Table 3 shows the values obtained from the uniaxial tensile test of PP bands in different modes,

Table 1. The specifications of the cement-sand mortar.

Parameter	Numerical value
Cement-sand ratio	1:6
Water-cement ratio	1:3
Compressive strength of mortar (MPa)	3.26
Shear strength from in-situ shear test (MPa)	0.15
Mean shear strength of the mortar from uniaxial test (MPa)	0.09

Table 2. Properties of bricks and masonry units (Coefficient of Variation is abbreviated as COV).

Type of brick	Property	Numerical value	COV (%)
Clay brick	Dimension (mm)	96 × 50 × 36	–
	Compressive strength (MPa)	5.7	17.3
	Water absorption (%)	15.9	18.7
	Modulus of elasticity (MPa)	1084	–
	Density (kN/m^3)	19.4	4.1
	Flexural strength (MPa)	1.29	11.4
Masonry unit	Compressive strength (MPa)	4.1	9.1

Table 3. Properties of the PP band.

Characteristics	Parameters	Mean	Standard deviation	No. of specimens
PP-band	Width (mm)	16	–	–
	Thickness (mm)	1.2	–	–
	Density (g/cm^3)	0.9	–	–
PP-band without punched clips	Tensile strength (MPa)	133.3	0.11	3
	Elastic modulus (GPa)	3.7	0.28	3
PP-band with punched clips	Tensile strength (MPa)	70.62	0.13	3
	Elastic modulus (GPa)	2.01	0.28	3

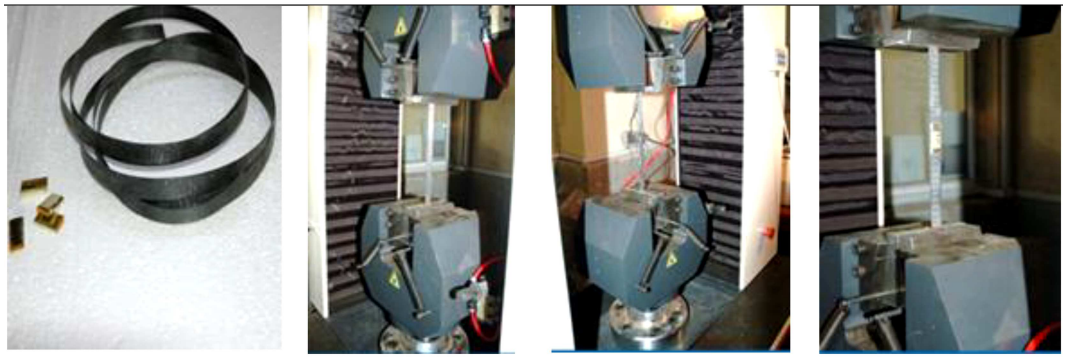

Figure 1. (a) PP band and clamp, (b) Uniaxial tensile test of the PP band, (c) Failure of to the PP band, and (d) Applying tension to the punched PP band with the clamp.

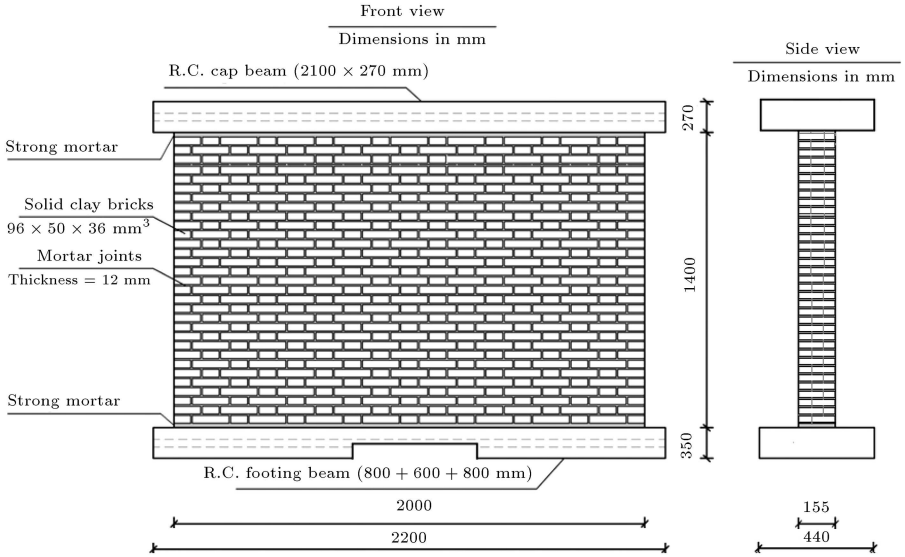

Figure 2. Schematic of the dimensions of the tested specimen.

which are in accordance with the standard [26]. In Figure 1(a), the PP band and metal clamp used in the uniaxial tensile test and the main masonry wall test are shown. In Figure 1(b), the PP band is stretched; in Figure 1(c), the PP band is tested until rupture. Figure 1(d) displays the PP-band tensile test with a metal clamp in the middle of the length according to what was mentioned in the previous section.

2.2. Geometry of specimens and test set-up

The test specimens consisted of three half-scale URM specimens of dimensions 2000 × 1400 × 155 mm (length × height × width). According to the literature available on an Iranian masonry construction [19,27], the wall dimensions with length of 2000 mm, height of 1400 mm, and wall thicknesses of 110 to 160 mm are common for the half-scale specimens, which have the same dimensions considered in the present study. Also, this gives an aspect ratio of 0.7 for the wall specimen. Besides, the width of the half-scale wall is taken herein as 150 mm, consisting of one brick 96 mm in length plus one brick 50 mm in width, on average. The first wall was subjected to cyclic quasi-static loading before and after the damage. Furthermore, having strengthened the second wall from the beginning, it was subjected to cyclic quasi-static loading. Above the tested masonry walls, there is a concrete beam with dimensions of 2100 × 270 × 440 mm, and at the bottom of the specimens, a concrete beam with dimensions of 2200 × 350 × 440 mm (length × height × width, respectively) is placed. As shown in Figure 2, the lower concrete beam is connected to the rigid floor with 8 pairs of high-strength screws with a nominal diameter of 20 mm and a length of 250 mm. In the stage of applying the reversed cyclic lateral load, two steel plates and four high-strength steel rebars with a diameter of 25.4 mm are used. According to Figure 2, a schematic of the specimen before the test and the dimensions of the wall and the number of rows of bricks are illustrated.

2.3. Instrumentation

According to Figure 3(b) and (c), two loadcells were

Figure 3. Stages of construction and instrumentation.

placed along the axle shaft of the hydraulic jack and the force distribution beam to measure the value of the applied lateral load. The third loadcell was used to control and measure changes in the vertical load during the experiment (Figure 3(h)). Furthermore, two LVDTs were used horizontally along the applied force to record the horizontal displacement, and the third LVDT was employed along the diameter of the specimen (Figure 3(c)–(e)). It should be mentioned that the upper and lower LVDT distances from the axis of the jackshaft are 21 and 14 cm, respectively. To control the out-of-plane movement of the wall and record the possible rotation period of the force distribution beam, the entire station with the surface accuracy of 1 mm (Figure 3(f)) and targets attached to the bottom, top, and middle of the wall height and, also, connected to the beam was used (Figure 3(g)). The camera operator read the mentioned points at peak moments of displacement and the beginning and end of each loading cycle. The data of the total station camera was utilized to control the movement of the upper concrete beam, which is responsible for distributing the load. As shown in Table 4, the camera and LVDT data are synchronized at the peak points of the loading pattern based on the point pick time, and significant consistency remains up to the tenth millimeter accuracy.

2.4. Loading protocol

The URMW were tested by applying an average constant vertical load of 28 kN concurrently with a quasi-static reciprocating cyclic lateral load recommended by the American Concrete Institute (ACI) [28]. At each drift ratio, three reciprocating cycles and half of the amplitudes were applied to the specimens. The initial drift ratio of the protocol is equal to 0.2%, at which the response interval of the fabricated specimens is linear. The axial distance of the lateral load is applied to the specimen at a height of 1535 mm above the foundation level. Figure 4 shows the lateral load protocol. A vertical load of about 2.8 tons should be applied to the specimen. A concrete beam with a weight of 6.9 kN and a vertical load of 21.03 kN was applied to the specimen. The stress resulting from the gravity load is

Table 4. Comparison between LVDT and survey data.

Time of observe	Survey data (mm)	Time of observe	LVDT (mm)	Max drift (%)	Cycle no.
05-03 16:07:17.0	−0.1720	03/05 16:02	−0.17	−0.008	1
05-03 16:13:53.0	−0.69	03/05 16:06	−0.67	−0.07	5
05-03 16:20:17.0	−0.912	03/05 16:19	−0.97	−0.1	8
05-03 16:32:56.0	1.792	03/05 16:30	1.77	0.14	9
05-03 16:57:19.0	−2.212	03/05 16:56	−2.41	−0.14	12
05-03 17:03:24.0	2.469	03/05 17:02	2.5	0.14	13
05-03 17:16:12.0	−2.745	03/05 17:15	−2.75	−0.14	14
05-03 17:44:19.0	−2.843	03/05 17:41	−2.09	−0.1	16
05-03 18:39:05.0	3.574	03/05 18:40	4.16	0.3	23
05-03 18:49:39.0	−4.285	03/05 18:46	−3.2	−0.28	24
05-03 19:01:34.0	−5.825	03/05 19:00	−5.7	−0.28	24
05-03 19:13:13.0	−4.579	03/05 19:11	−4.7	−0.28	24
05-03 19:43:12.0	6.455	03/05 19:42	6.58	0.34	25
05-03 20:02:38.0	−0.035	03/05 20:02	0	−0.008	29

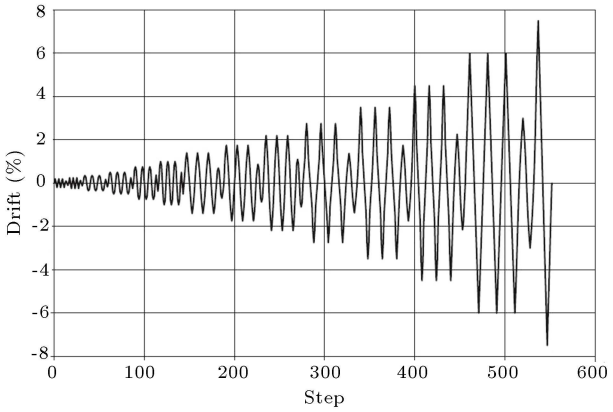

Figure 4. Cyclic load protocol.

calculated as 0.75 MPa. In order to load vertically, a manual hydraulic jack was used on the concrete beam.

2.5. Details of the proposed strengthening technique

In the proposed method for repairing and retrofitting, the materials used in both cases are plastic products with a low price and worldwide availability. The methodology and concept of repairing and strengthening the masonry wall in any damaged condition and before the damage are closely related. The first involves repairing the damaged wall with such goals as using minimum manpower, materials for repair, and technical skills of the expert force as well as the best possible efficiency, improving seismic performance, stopping the crack pattern, and finally preventing wall destruction. Second, PP fibers, even with the worst quality available, enjoy much higher tensile strength than cement-sand mortar. The technique of improvement with PP fibers should be applied in the fastest possible time and in this respect, the improved structure can protect the residents who are temporarily staying in it from the aftershocks and so on. To this end, the strengthening technique must be employed during the fiber loading in question (PP fibers can be fastened in different forms around the wall: horizontal strap, vertical strap on the sides, alternate vertical and horizontal bands, i.e., warps and wefts, and also fibers along the diameter of the wall or oblique fibers, etc.). Since strap fastening is placed in the thickness of the wall and each strap has only one fastening along the wall, the amount of force applied to fasten the strap around the wall is very small to the extent that the strap touches the wall surface. On the other hand, the strength of the PP strap is low (100 kg fastened strap) and since the bands did not rupture in the experiments, the initial condition of the bands lacks considerable force (Figure 5(a) and (b)). In the tested specimen, the walls were only retrofitted with PP fibers horizontally in order to strengthen the wall (Figure 5(c)). In the areas of the wall where cracks have formed at a depth of the wall, the bands are fastened to each other with the help of wire on both sides of the wall and are completely tangent to the wall surface to achieve the best performance (Figure 5(d)). As for real and full-scale structures, the proposed method can be utilized on site. In doing so, a few holes are required to be drilled through the wall thickness and within the weak mortar layer in order to pass the steel wires to connect

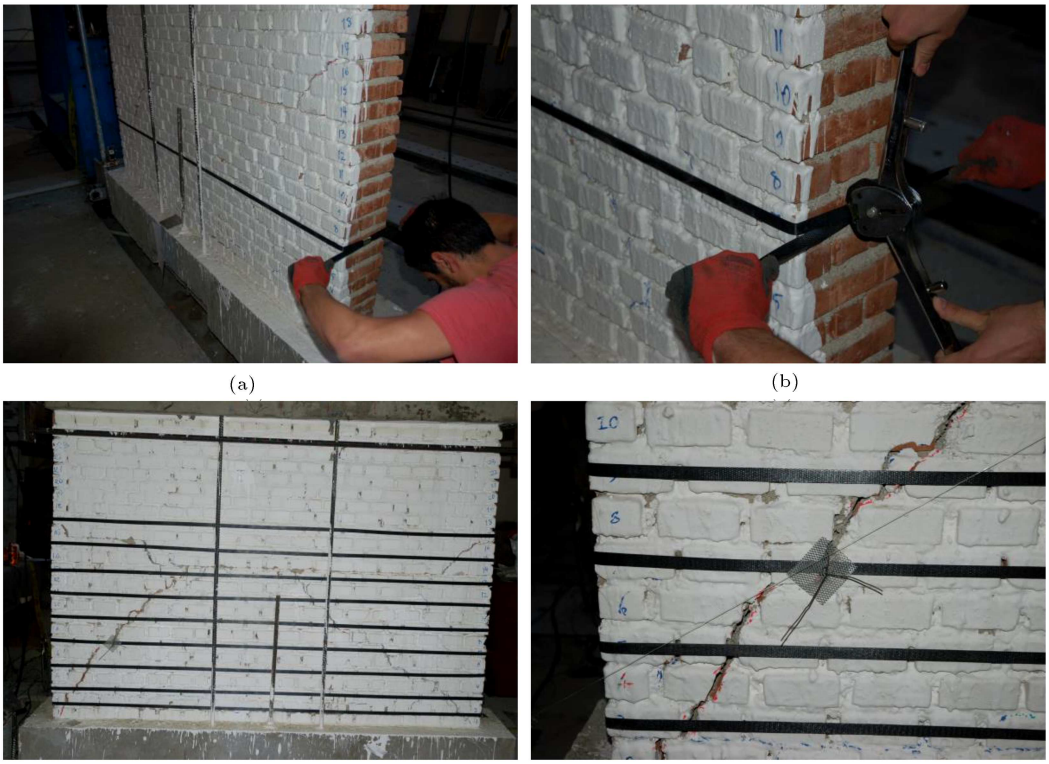

Figure 5. The process of repairing the damaged masonry wall.

and fix the PP bands on both sides of the wall (in the case of repairing the damaged wall), or to pass the PP bands near the wall ends to encircle the wall thickness (in the case of strengthening the existing wall). In the latter case, a mortar layer is shotcrete on the wall surface to cover the PP bands and also, to provide better attachment for the PP bands to the masonry wall surface. When strengthening, the PP bands may be anchored into a small cement foundation built at the bottom of the wall.

The third point concerns strengthening the masonry wall before loading. Due to the similarity of the manufacturing process and the same dimensions, mortar thickness, ratio of sand to cement, and loading pattern, it is not at all far-fetched to predict similar behavior. Therefore, using a similar and expanded process, the next specimen was reinforced before applying lateral load and wall damage. To reinforce the specimen, the PP fibers are used in horizontal, vertical, and oblique positions (Figure 6(c)). The horizontal bands in each row are fastened alternately on the levels of the bricks, and three vertical bands are fastened at a distance of 30 cm from the end of the wall (on both sides of the wall and like a vertical coil). The way the oblique bands are fastened is based on the crack pattern created in the first specimen test with the aim of preventing the spread of cracks. By dividing the length and height of the wall into three equal parts, oblique bands are used to strengthen the wall (Figure 6(a)). It is necessary to enclose and attach the bands to the wall in order to engage the bands when loading in low drifts (Figure 6(b)). In order to enclose the bands, a cement-sand mortar layer (similar to the horizontal mortar used in building the wall) was coated on the bands with an average thickness of 20 mm (Figure 6(d)). In order for the coating to have minimal effect on the behavior of the wall, given that the most influential factor in the improvement of the wall is the use of PP bands, the coated surface should be as small as possible. On the other hand, this surface should provide enclosure and integration of the bands with walls (Figure 6(e)).

3. Experimental observations

During the experiment, various observations were recorded, which would be discussed and presented in this section.

3.1. Unreinforced Masonry Wall (URMW)

The first crack in the 0.05% drift was observed below the fourth row of the wall with a horizontal crack length of 40 cm. (Figure 7(a)) In the continuation of the experiment up to 0.2% drift, vertical and horizontal cracks consisting of toes were connected to each other; hence, they caused the diagonal crack pattern to be observed from the toe to the bottom of the brick of row 15. According to the lateral loading pattern

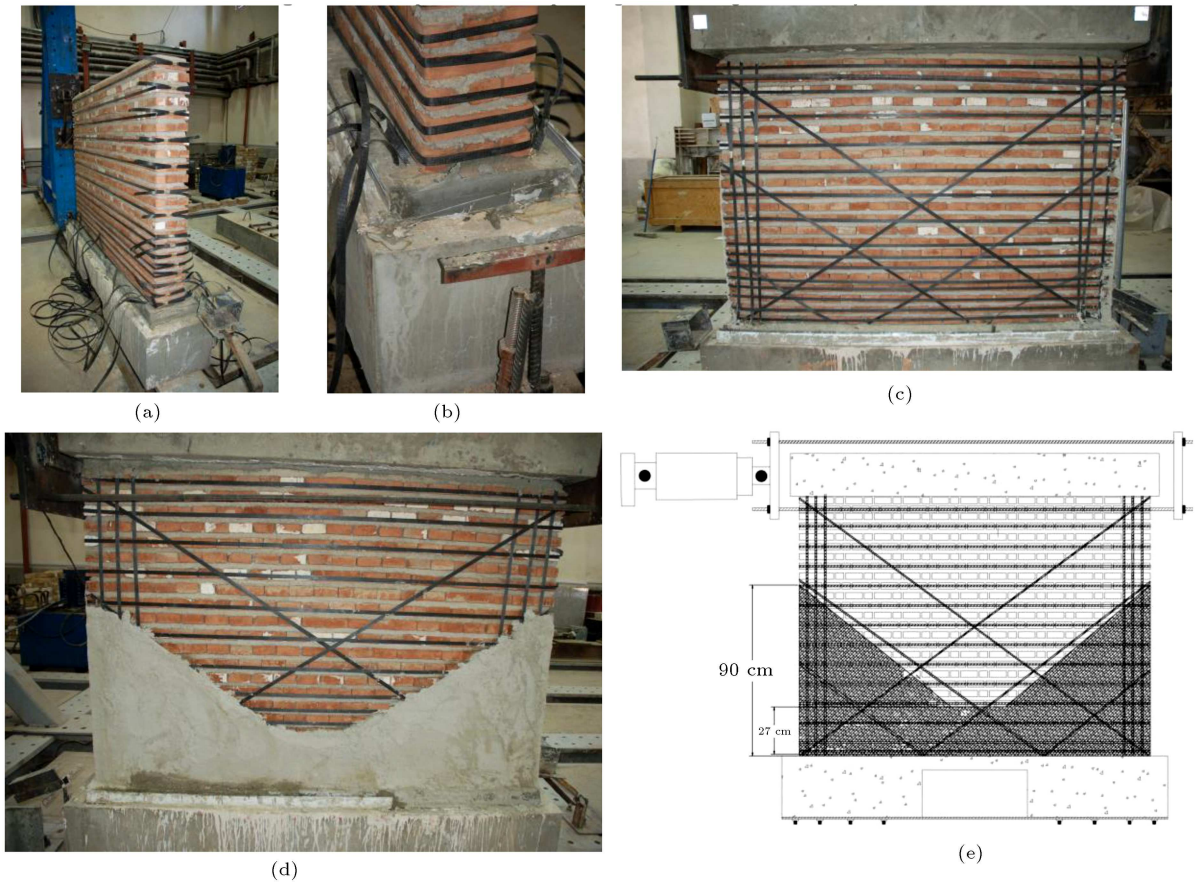

Figure 6. The process of strengthening the unreinforced masonry wall.

applied to the test specimen up to 0.3 drift in the toe areas as well as the lower rows of the specimen on the footing, horizontal cracks with large lengths were formed in the specimen. These cracks were in the form of capillaries and as the experiment continued, these cracks did not expand and practically, the failure mode of the specimen was not formed because of these capillary cracks (Figure 7(b)). At a displacement of +4.29 mm (equivalent to 0.3% drift), a horizontal crack along the length of a brick began from the side of the jack under row 17 (Figure 7(c)), entered the horizontal mortar below row 16 by passing through a brick with a stepped position, and continued horizontally again with a stepping mode between rows 13 and 14 (Figure 7(d)). A deep horizontal shear crack was developed at half the height of the wall along the entire length of the wall, and the dominant failure mode could certainly be considered a result of the formation of this shear-slip crack. Moreover, at a displacement of +5.6 mm (equivalent to 0.4% drift), vertical cracks were created and with the connection of vertical and horizontal cracks, up to the horizontal crack between rows 13 and 14, a continuous diagonal crack was observed (Figure 7(e)). At a 0.43% drift, the applied lateral load caused the spread of diagonal cracks to the lower part of the shear-slip crack, which formed a connection between these diagonal cracks and the horizontal crack in question (Figure 7(f)).

3.2. Retrofitted Damaged Masonry Wall (RDMW)

In the loading test of the horizontal PP strap-reinforced damaged masonry wall, the principle that each strap was operating independently in the row to which it was fastened was observed. Each strap dissipated energy by keeping the wall cohesive and allowing rows of bricks to slide on top of each other (Figure 8(a)). During loading at a 0.8% drift, the widths of the cracks were set to 21 mm, and the horizontal slip between rows 13 and 14 was reported to be 14 mm (Figure 8(b)). Sliding wall layers on each other caused horizontal cracks to penetrate deep into the wall, and the cracks were visible on both sides of the wall. At the end of the experiment, between rows 14 and 15, the wall made a 2 cm torsional motion towards the external side of the wall plate and the lateral load axis and a horizontal residual slip of 5 cm was recorded (Figure 8(c)–(e)).

3.3. Strengthened Unreinforced Masonry Wall (SUMW)

The first crack was observed at a displacement of +1.62 mm on both sides of the wall at a height of

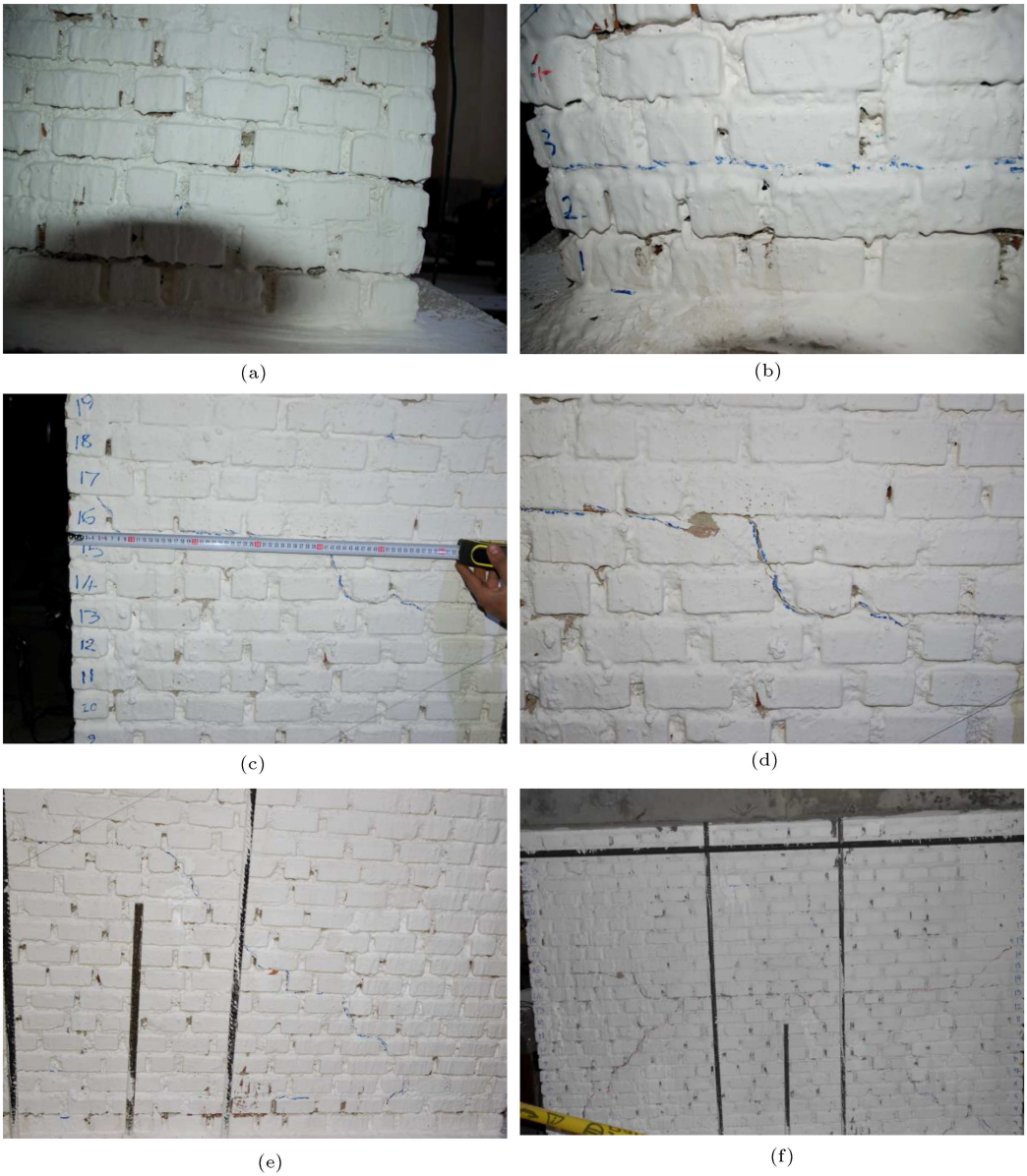

Figure 7. The unreinforced masonry wall experiment.

27 cm from the level on the foundation with a length of 72 cm horizontally; and at a 0.15% drift, the crack length increased to 120 cm (Figure 9(a) and (b)). At a displacement of +2.8 mm, a horizontal crack of 120 cm at a height of 27 cm continued diagonally and down the wall with an oblique length of 25 cm to the foundation. At a −2.1 mm displacement of the horizontal crack on the level of the foundation, a horizontal crack with a length of 147 cm was formed. At a 0.14% drift, the crack on the level of the foundation increased to a length of 160 cm. Below the level of the foundation, a horizontal crack of 45 cm length parallel to the top crack was formed on both sides of the wall (Figure 9(c)). At a 0.28% drift in the toe of the wall, a vertical crack with a height of 5 cm appears on both sides of the wall. At a 0.6% drift, diagonal cracks and cement coat debonding were observed in the toes, and the wall uplifting was recorded as 9 mm from below the foundation (Figure 9(h)), which was observed along the wall and on both sides (Figure 9(g)). No significant change was observed in the crack pattern at a 1% drift at the end of the experiment except for increased debonded areas and toe crushing when the wall experienced a displacement equivalent to 1.6% drift (Figure 9(e)). At a 1% drift, in the toe and a domain with a length of 20 cm and a height of 8 cm, toe crushing occurs. At positive and negative maximum displacements, two rectangle-like areas in both toes with dimensions that are 20 to 25 cm in the length and 15 to 20 cm in the height of the wall are crushed (Figure 9(d)). At the maximum displacement of +19.6 mm, the horizontal crack formed at a level of

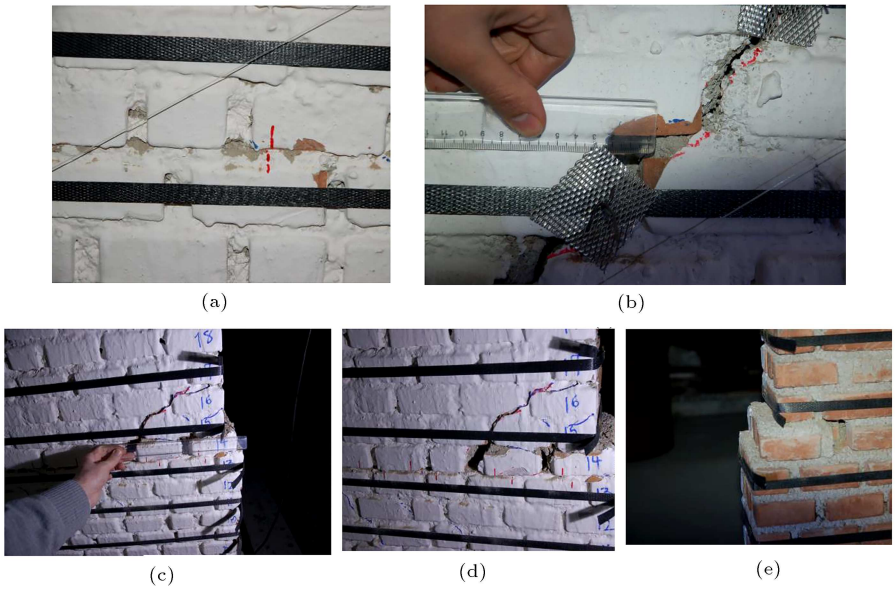

Figure 8. The damaged masonry wall experiment.

26 cm from the foundation was completely closed, and the uplifted length and the width of the crack under the foundation were reported as 120 cm and 26 mm, respectively (Figure 9(f)). At a −9 mm displacement, the wall underwent a horizontal slip of 10 mm in the direction of the force (Figure 9(i)).

4. Experimental results and discussion

This section demonstrates the experimental results of the reference specimen or the URMW, the retrofitted damaged specimen, and the strengthened undamaged specimen. In addition to the description, the crack pattern, hysteresis curve, stiffness, strength, and dissipated energy are compared. Table 5 indicates the maximum bearing capacity, ultimate strength, and the maximum lateral displacement of the un-strengthened specimen, strengthened damaged specimen, and the strengthened specimen.

4.1. Crack pattern and hysteresis curve

According to the observations, the reference specimen exhibited linear behavior up to 0.05% drift and no crack was observed in the wall. The first crack was observed at a displacement of +0.7 mm at a lateral force of 10.02 kN. Then, with increasing lateral load to drifts less than 0.1%, horizontal cracks formed in one-third of the bottom of the wall and in the toes. In short, from 0.1% to 0.2% drift, the most obvious occurrence is the emergence of vertical cracks and the formation of a stepped state due to the connection of these cracks to the horizontal cracks that were created in previous cycles. In other words, diagonal cracks were formed due to the connection of vertical and horizontal cracks which appeared at the height of one-third of the bottom of the wall. After a 0.3% drift, a shear crack was developed along the entire wall, and with the beginning of cycle 12 at a drift of 0.4%, a deep horizontal crack appeared in half the height of the wall along the entire

Table 5. The results of the idealization of specimens.

Specimens' ductility parameters							
Backbone curve	Lateral stiffness	Yield condition		Ultimate condition		Elastic displacement d_e (mm)	Ductility $\mu = d_u/d_e$
	Initial stiffness K_i (kN/mm)	Lateral load V_y (kN)	Displacement d_y (mm)	Lateral load V_u (kN)	Displacement d_u (mm)		
		Unreinforced masonry wall					
Average	25.92	13.05	0.64	15.66	6.61	0.768	8.6
		PP-retrofitted damaged masonry wall					
Average	25.92	11.19	0.64	13.41	13.48	0.764	–
		PP-retrofitted masonry wall					
Average	25.01	28.37	1.62	34	21.15	1.94	10.9

Figure 9. The strengthened masonry wall experiment.

wall, which can certainly be considered the dominant failure mode due to the formation of this shear-slip crack. At a displacement of 5.85 mm, in addition to increasing the width of the crack under study, diagonal cracks spread to the lower part of the shear-slip crack, which led to the formation of a connection between vertical and horizontal cracks, and the cracks from the toes were connected to develop a diagonal crack pattern from the toe to under the brick in row 15. The experiment continued until a drift of 0.48%. With a 28% drop in bearing capacity, the test sample was stopped.

In order to investigate the effect of PP bands on the performance of the damaged wall, the URMU was loaded up to 0.48% drift and more than 0.35% for damage with the moderate amount recommended in FEMA 306 [29].

With the help of fastened horizontal bands, the spread of the crack pattern was stopped. Also, the lateral bearing capacity of the specimen up to 0.38% drift with a drop of 9% was almost equal to the lateral capacity of the prototype. Testing of the retrofitted damaged specimen continued up to 1.4% drift. In the strengthened masonry wall, no crack was observed up to 0.081% drift and in the lateral force of 28.32 kN, and the effect of strengthening besides increasing the bearing capacity in improving the elastic behavior of the masonry wall was also evident. The failure mode

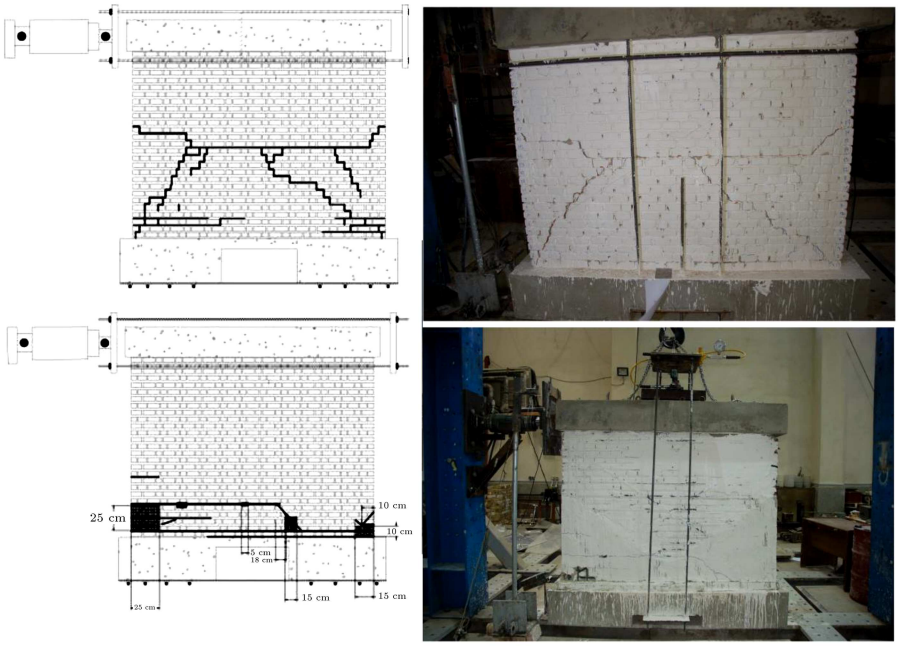

Figure 10. Comparison of the crack patterns of the URMW and SUMW.

of the un-strengthened specimen began with the first crack and the spread of the diagonal-tensile crack pattern, and in the 0.48% drift, the shear-slip failure mode was created in the specimen, and the failure mode of the specimen was considered as a combination of the two main in-plane modes. The failure mode of the strengthened specimen was rocking motion, and at a 1.6% drift, a crack was created in the toe of the wall and a layer of cement-sand coating was on the verge of separation from the specimen surface. The crack pattern of the reference and strengthened specimens at the end of the experiment where the wall experienced a displacement equivalent to 1.6% drift is shown in Figure 10. The hysteresis curves of the three specimens are illustrated in Figure 11. In a sound retrofitted masonry wall, non-slip horizontal cracks, preventing the cracks from opening and closing by horizontal and oblique bands as well as enclosing them with the applied mortar, reduce the size of cyclic curves. Figure 11(a)–(d) shows the hysteresis curves of the reference, retrofitted damaged, and strengthened specimens as well as the comparison of all the three curves.

4.2. Idealization process of the actual structural response curve

In order to further evaluate the behavior of the specimens, in addition to the cyclic curve, an equivalent bilinear force-displacement curve is considered. The bilinear curve [30] is the idealized format of the envelope diagram for the experimental cyclic curve of the specimen, expressing a relationship between the base shear and the displacement at top of the wall, as depicted in Figure 12.

The main parameters of a bilinear curve include effective lateral stiffness (K_e), maximum shear force (V_u), and displacement (d_e) at the intersection between two lines in the bilinear curve, as depicted in Figure 13. Besides, the maximum or ultimate displacement (d_u) is defined as the displacement corresponding to a 20% drop in the maximum lateral capacity of the experimental curve (i.e., 0.8 $V_{\max}$) [31], as illustrated in Figure 12.

$$V_u = 0.8V_{\max} \qquad d_u = d_{0.8V_{\max}}, \tag{3}$$

where K_e is the effective lateral stiffness and is defined as the secant slope calculated for the shear equal to $0.7V_{\max}$. In addition, A_{env} indicates the area enclosed under the envelope curve in a positive or negative region. The parameters of the equivalent bilinear force-displacement curve are calculated using the following equations [32]:

$$V_u = K_e\left(d_{\max} - \sqrt{d_{\max}^2 - \frac{2A_{env}}{K_e}}\right), \tag{4}$$

$$V_u = 0.84V_{\max}, \tag{5}$$

$$k_e = \frac{V_{cr}}{d_{cr}}, \tag{6}$$

$$d_e = \frac{V_u}{K_e}, \tag{7}$$

$$\mu = \frac{d_u}{d_e}. \tag{8}$$

According to the study in [27], the initial stiffness of the masonry walls subjected to lateral loading

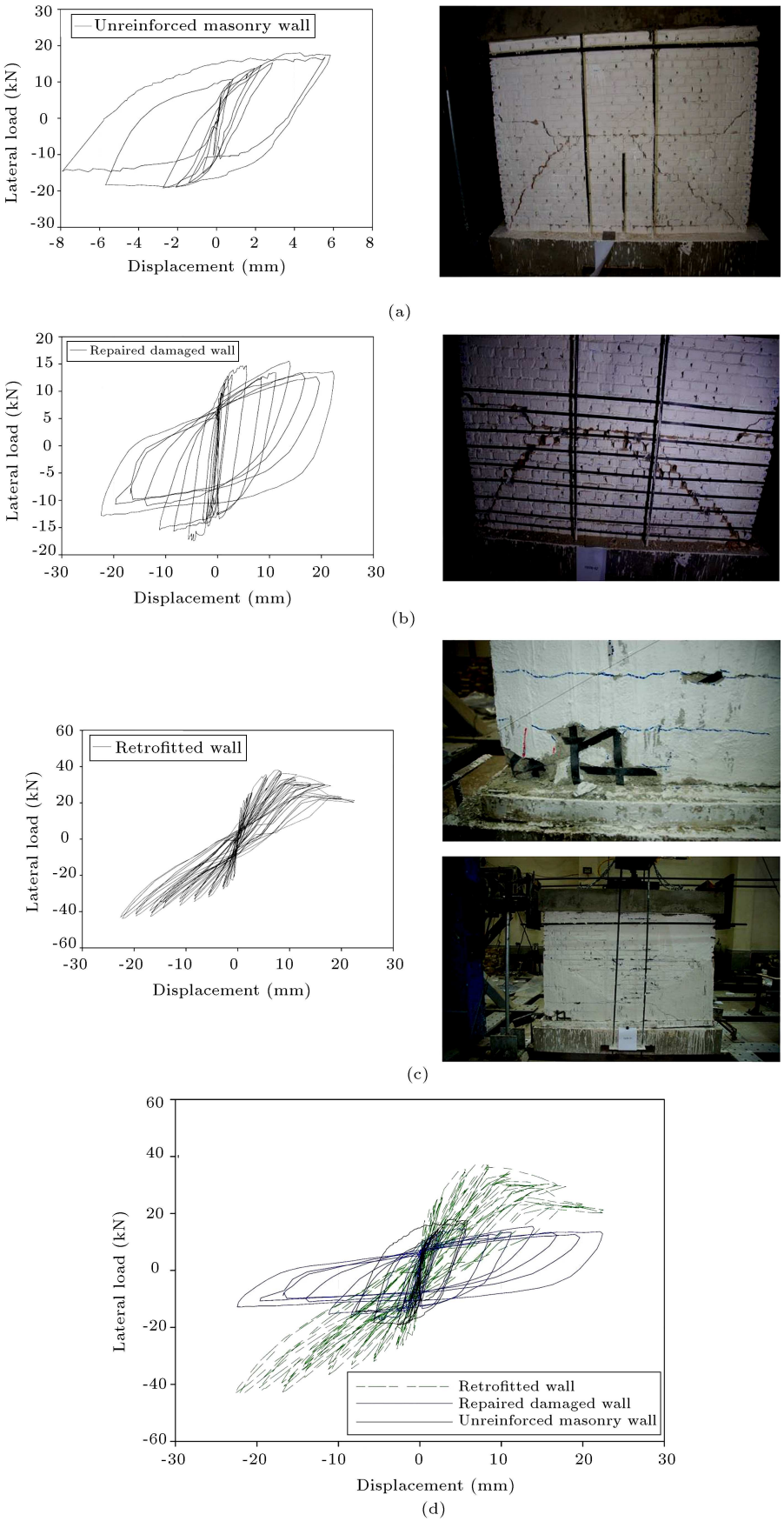

Figure 11. Hysteresis curves of the experimental specimens.

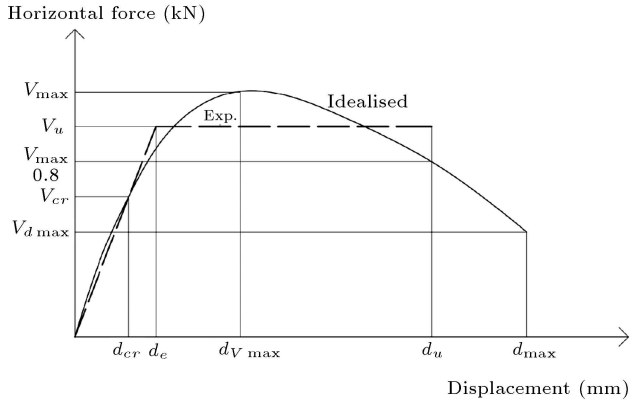

Figure 12. Actual and idealized response envelopes [31].

could be measured when the wall behaves in the elastic region. In this regard, the initial stiffness, K_i, is defined as the tangent slope of the experimental envelope curve at the origin point. Alternatively, the initial stiffness can be estimated as the secant slope of the experimental curve corresponding to a 0.1% drift ratio. According to the data extracted from the bilinear force-displacement curve reported in Table 6, the maximum strength and ultimate strength of the retrofitted damaged specimen decreased by 26% and 13%, respectively, compared to the prototype. The maximum displacement of the retrofitted damaged specimen is 183% greater than that of the prototype. Moreover, the maximum strength, ultimate strength, and maximum displacement of the retrofitted specimen increased by 88%, 38%, and 185%, respectively, compared to the un-strengthened specimen. The retrofitted damaged specimen has the lowest ultimate strength among the three specimens, and its final lateral displacement is 171% greater than that of the un-strengthened specimen. Therefore, the effect of the proposed technique on improving the performance of walls is herein pronounced. By retrofitting the damaged wall, the lateral capacity does not increase significantly and even, the stiffness of the wall decreases compared to the unreinforced state, but the ductility and the maximum lateral displacement have increased significantly. Increased ductility has led to an increase in the energy dissipation capacity of the specimens, which is of importance for unreinforced masonry walls.

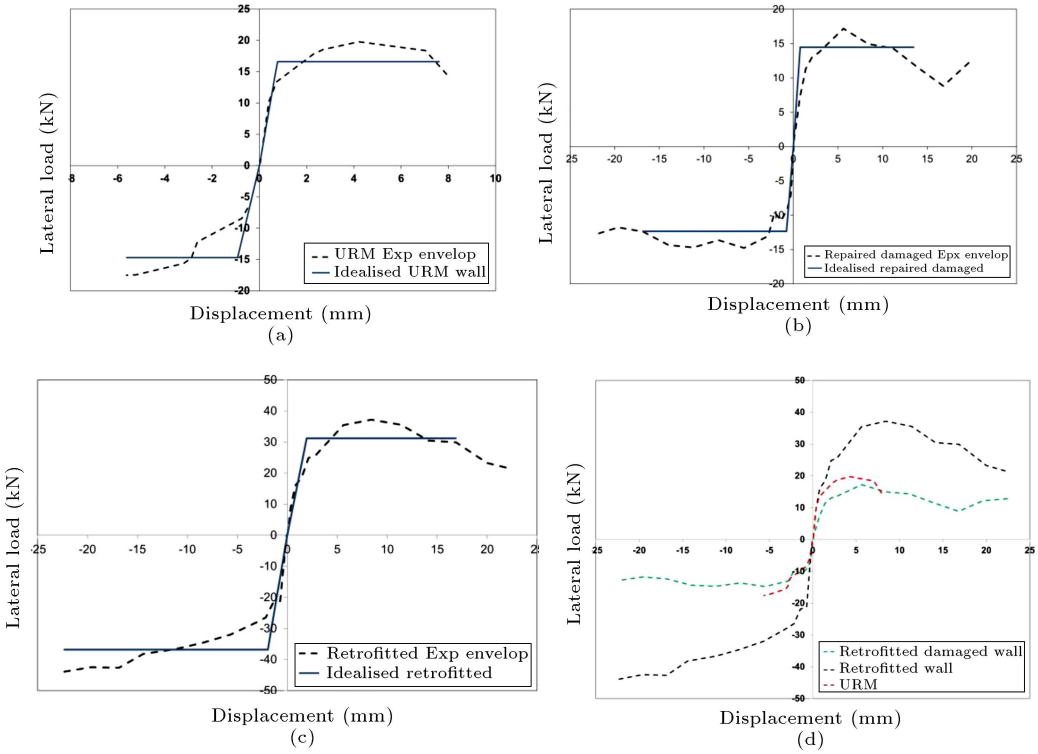

Figure 13. Idealized load-displacement curve of specimens.

Table 6. Comparison of calculated and experimental results of shear capacity.

	Experimental shear strength (kN)	Calculated shear strength (kN)	Ratio
Strengthened specimen	37.16	32.38	0.87

5. Prediction of shear capacity

5.1. Predictive equation

In this section, according to the experimental observations and the obtained results, an equation is proposedto predict the shear strength of the masonry wall reinforced with PP band and cement-sand coating. Considering the behavior of the sample during the test and the conditions of connection of PP bands to the masonry wall from the top beam to the foundation of the wall floor and the integrity of the whole tested sample as a composite element, this equation has been suggested. It should be noted that the reinforced wall is modeled as a composite body that includes two parts of the building unit and materials used for reinforcement, which are PP and cement. As shown in Figure 14, H_1 is the wall height (1400 mm) and $M_{\max}$ is the maximum bending moment that is resistant to lateral force. According to the basic assumption of the bending theory in which the plane remains flat after bending, the crack threshold strain value can be considered equal for both defined elements. In the proposed equation, the bending capacity of the wall is calculated based on ε_{tu}, and the final tensile strain of the bands is 0.1. Also, the final compressive strain of the reinforced wall is less than the strain obtained from the strength test of prismatic sample materials. In the proposed equation, the bending capacity of the wall is calculated based on the final tensile strain of the bands. In addition, in practice, the final compressive strain of the reinforced wall is less than the strain obtained from the strength test of prismatic sample materials. In the presented equation, t_c is the thickness of mortar and PP band with decreasing coefficient (less than 20 mm and equal to 10 mm), t_m is wall thickness (200 mm), and L_w is the effective wall length or 0.8 actual length of the wall (1600 mm). Regarding other parameters of this equation, N is axial force (21.03 kN), f_t is the tensile stress with decreased coefficient in order to consider the effect of mortar and PP together ($\approx 0.2 \times 133.3 = 26.6$ MPa), f_{tu} is the ultimate tensile stress, E is the modulus of elasticity of the reinforcement material (3.7 GPa), and E_m is the modulus of elasticity of the material ($1000 \times f_m$). According to masonry characteristics, two other important assumptions have been applied to the fundamental bending relationship. First, the value of T_2 in the linear range is much less than that of T_1; thus, it is omitted. Moreover, the tensile strength of the masonry wall was neglected during the test, and all tensile strengths were attributed to the reinforcement materials. It is noted that the PP bands embedded in the mortar layer covering the wall surface are treated as a composite material, which develops compressive strength through the mortar layer while providing the tensile capacity by the PP band. Following this analogy, P_1 and T_1 represent the resultant forces related to compression and tension, respectively, acting on the wall cross-section. On the other hand, the masonry units provide compression (denoted by P_2), whereas the tensile contribution by the masonry units is ignored.

$$V_{\max} = \frac{M_{\max}}{H_1} = 32.387 \text{ kN}, \tag{9}$$

$$M_{\max} = f_t \times t_c \left(L_w - x_1\right) \times \left(0.5L_w - \frac{x_1}{6}\right) + (0.5L_w - x_1) \times N = 45.3431 \text{ kN.m}, \tag{10}$$

$$x_1 = \frac{N + f_t \times t_c \times L_w}{0.5 \times (E \times t_c + E_m \times t_m) \times \varepsilon_c + f_t \varepsilon_{tu} t_c} = 0.188 \text{ m}. \tag{11}$$

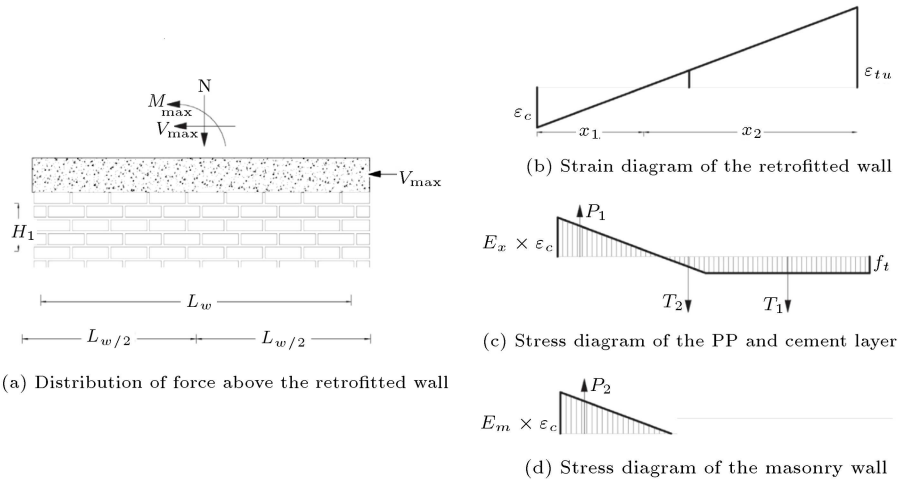

(a) Distribution of force above the retrofitted wall

(b) Strain diagram of the retrofitted wall

(c) Stress diagram of the PP and cement layer

(d) Stress diagram of the masonry wall

Figure 14. Retrofitted specimens stress-strain diagram and forces distribution corresponding to the bending capacity.

Table 7. Summary of the test results.

	Maximum strength (kN)	Ultimate strength (kN)	Maximum displacement (mm)
Un-strengthened specimen	19.77	14.63	7.92
Strengthened damaged specimen	14.55	12.8	22.42
Strengthened specimen	37.16	20.25	22.64

5.2. Comparison of the calculated and measured shear capacities

A comparison between the test results and the proposed relationship is presented in Table 7. As seen in the last column (Table 7), the difference is approximately 13.13%.

6. Conclusion

This study conducted an experimental program to investigate the performance of the PP band in repairing and retrofitting of an unreinforced masonry walls. The results of the investigation are as follows:

- The maximum strength and ultimate strength of the retrofitted damaged specimen decreased by 26% and 13%, respectively, compared to the prototype. The maximum displacement of the retrofitted damaged specimen is 183% greater than that of the prototype;
- Reinforcement of the damaged specimen prevented the decrease of lateral bearing capacity, and the lateral bearing capacity of the specimen up to 0.38% drift with a 9% reduction was almost equal to the lateral capacity of the prototype. At a 1.2% drift, the bearing capacity decreased by 23% and before the drift in question, the changes in the bearing capacity of the strengthened damaged specimen were small;
- In the unreinforced wall, horizontal and vertical cracks were observed, connected to each other with increasing lateral displacement. The unreinforced damaged masonry wall had a larger cyclic curve due to the possibility of sliding rows of bricks along the crack. Thus, the strength of the retrofitted damaged masonry wall could dissipate energy up to 23% more than the strengthened specimen and 60% more than the unreinforced masonry wall;
- To strengthen the damaged specimen, polypropylene bands were used only horizontally and according to the failure mode of the prototype, which is a combination of diagonal-tensile mode and shear-slip failure;
- The maximum strength, ultimate strength, and maximum displacement of the retrofitted specimen increased by 88%, 38%, and 185%, respectively, compared to the unreinforced masonry wall;
- The shear and tension-diagonal failure mode of the unreinforced masonry was as expected. With the retrofitting method, the failure mode changed, which was also an important and desirable result of the test. Since the ratio of height to the length of the wall was less than 1, the retrofitted and unretrofitted walls show two different failure modes. It is worth mentioning that the prevailing mode changed from shear to flexural (rocking);
- The ductility coefficient of the strengthened masonry wall is 26% higher than that of the unreinforced masonry wall;
- According to the equivalent two-line force-displacement curve, the mean values of the ultimate strength and the corresponding displacement in the retrofitted damaged specimen had the lowest ultimate strength among the three specimens. The ultimate strength and ultimate lateral displacement of the strengthened specimen were 171% and 196% higher than the unreinforced masonry wall, respectively.

Nomenclature

V_{test}	The force obtained from the in-situ shear test
V_{to}	Shear stress; that the average of the tested amounts is placed in Eq. (2)
A_b	The surface of the upper and lower horizontal mortar
A_n	Mortar net area
K_e	Effective lateral stiffness
V_u	Maximum shear force
d_e	Displacement
d_u	Maximum displacement
A_{env}	The area under the envelope curve in the positive or negative regions
H_1	Wall height
t_c	Thickness of mortar and PP strap with decreasing coefficient
t_m	Wall thickness
L_w	Effective wall length
N	Axial force
f_t	Tensile stress with decreased coefficient

f_{tu}	Ultimate tensile stress
E	Modulus of elasticity of the reinforcement material
E_m	Modulus of elasticity of the material

References

1. Ghiassi, B., Soltani, M., and Tasnimi, A.A. "Seismic evaluation of masonry structures strengthened with reinforced concrete layers", *Journal of Structural Engineering*, **138**(6), pp. 729–743 (2012).
2. Kadam, S.B., Singh, Y., and Li, B. "Strengthening of unreinforced masonry using welded wire mesh and micro-concrete-Behaviour under in-plane action", *Construction and Building Materials*, **54**, pp. 247–257 (2014).
3. Shermi, C. and Dubey, R.N. "Study on out-of-plane behaviour of unreinforced masonry strengthened with welded wire mesh and mortar", *Construction and Building Materials*, **143**, pp. 104–120 (2017).
4. Wang, C., Sarhosis, V., and Nikitas, N. "Strengthening/retrofitting techniques on unreinforced masonry structure/element subjected to seismic loads: A literature review", *The Open Construction and Building Technology Journal*, **12**(1), pp. 251–268 (2018).
5. Reboul, N., Mesticou, Z., Larbi, A.S., et al. "Experimental study of the in-plane cyclic behaviour of masonry walls strengthened by composite materials", *Construction and Building Materials*, **164**, pp. 70–83 (2018).
6. Ismail, N., El-Maaddawy, T., and Khattak, N. "Quasi-static in-plane testing of FRCM strengthened non-ductile reinforced concrete frames with masonry infills", *Construction and Building Materials*, **186**, pp. 1286–1298 (2018).
7. Niasar, A.N., Alaee, F.J. and Zamani, S.M. "Experimental investigation on the performance of unreinforced masonry wall, retrofitted using engineered cementitious composites", *Construction and Building Materials*, **239**, 17788 (2020).
8. Wang, F., Kyriakides, N., Chrysostomou, C., et al. "Experimental research on bond behaviour of fabric reinforced cementitious matrix composites for retrofitting masonry walls", *International Journal of Concrete Structures and Materials*, **15**(1), pp. 1–17 (2021).
9. Carozzi, F.G., Milani, G., and Poggi, C. "Mechanical properties and numerical modeling of Fabric Reinforced Cementitious Matrix (FRCM) systems for strengthening of masonry structures", *Composite Structures*, **107**, pp. 711–725 (2014).
10. Gattesco, N. and Boem, I. "Characterization tests of GFRM coating as a strengthening technique for masonry buildings", *Composite Structures*, **165**, pp. 209–222 (2017).
11. Kassem, N., Atta, A., and Etman, E. "Structural behavior of strengthening masonry in-filled frames subjected to lateral load using bonded and un-bonded CFRP", *KSCE Journal of Civil Engineering*, 21(3), pp. 818–828 (2017).
12. Yacila, J., Salsavilca, J., Tarque, N., et al. "Experimental assessment of confined masonry walls retrofitted with SRG under lateral cyclic loads", *Engineering Structures*, **199**, 109555 (2019).
13. Nayak, S., Banerjee, S., and Das, S. "Augmenting out-of-plane behaviour of masonry wallet using PP-band and steel wire mesh", *IOP Conference Series: Materials Science and Engineering* (2018).
14. Heydariha, J.Z., Ghaednia, H., Nayak, S., et al. "Experimental and field performance of PP band-retrofitted masonry: evaluation of seismic behavior", *Journal of Performance of Constructed Facilities*, **33**(1), 04018086 (2019).
15. Banerjee, S., Nayak, S., and Das, S. "Improving the in-plane behavior of brick masonry wallet using PP Band and steel wire mesh", *Journal of Materials in Civil Engineering*, **32**(6), 04020132 (2020).
16. Meguro, K., Mayorca, P., Sathiparan, N., et al. "PP-Band retrofitting technique: Affordable, acceptable and feasible method for developing countries", *Institute of Industrial Science*, University of Tokyo (2005).
17. Nissanka, N.A.A.C., Priyankara, R.L.S., and Sathiparan, N. "Comparison of mesh type seismic retrofitting for masonry structures", *3rd International Symposium on Advances in Civil and Environmental Engineering Practices for Sustainable Development*, Galle, Sri Lanka, pp. 334–341 (2015).
18. Macabuag, J., Guragain, R., and Bhattacharya, S. "Seismic retrofitting of non-engineered masonry in rural Nepal", *Proceedings of the Institution of Civil Engineers-Structures and Buildings*, **165**(6), pp. 273–286 (2012).
19. Mansouri, A., Marefat, M.S., and Khanmohammadi, M. "Experimental evaluation of seismic performance of low-shear strength masonry infills with openings in reinforced concrete frames with deficient seismic details", *The Structural Design of Tall and Special Buildings*, **23**(15), pp. 1190–1210 (2014).
20. ASTM C109/C109M-16a, Standard Test Method for Compressive Strength of Hydraulic Cement Mortars (Using 2-in. or [50-mm] Cube Specimens), ASTM 2016 International, West Conshohocken, PA 10.1520/C0109-C0109M-16A.
21. ASTM C109/C109M-16a, Standard Test Method for Compressive Strength of Hydraulic Cement Mortar (Using 2-in. or [50-mm] Cube Specimens), ASTM 2016 International West Coshohocken, PA 10.1520/C0109-C0109M-16A.

22. FEMA 306, Evaluation of Earthquake-Damaged Concrete and Masonry Wall Buildings-Basic Procedures Manual, prepared by the Applied Technology Council (ATC-43 Project), for the Federal Emergency Management Agency, Washington, D.C. (1998).

23. ASTM C67-1995, Standard Test methods for Sampling and Testing Brick and Structural Clay.

24. ASTM D2216-19, Standard Test Methods of Laboratory Determination of Water (Moisture) Content of Soil and Rock by Mass, ASTM International, West Conshohocken, PA, 2019, DOI:10.1520/D2216-19.

25. ASTM C1314-18, Standard Test Method for Compressive Strength of Masonry Prisms, ASTM International, West 2018 Conshohocken; PA 10,1520/C1314-18.

26. ASTM D3039/D3039M-17, Standard Test Method for Tensile Properties of Polymer Matrix Composite Materials, ASTM 2017 International, West Conshohocken, PA 10.1520/D3039-D3039M-17.

27. ACI Innovation Task Group 1 and Collaborators. Acceptance Criteria for Moment Frames Based on Structural Testing. ACI T1.1-01. American Concrete Institute: Farmington Hills, MI (2001).

28. FEMA306, Evaluation of earthquake damaged concrete and masonry wall buildings (basic procedure manual), Federal Emergency Management Agency, Washington, DC. (1998).

29. Tomazevic, M. "Earthquake-resistant design of masonry buildings", (**1**). World Scientific Publishing, Singapore (1999).

30. Park, R. "Evaluation of ductility of structures and structural assemblages from laboratory testing", *Bulletin of the New Zealand Society for Earthquake Engineering*, **22**(3), pp. 155–166 (1989).

31. Magenes, G. and Calvi, G.M. "In-plane seismic response of brick masonry walls", *Earthquake Engineering and Structural Dynamics*, **26**(11), pp. 1091–1112 (1997).

32. Darbhanzi, A., Marefat, M.S., and Khanmohammadi, M. "Investigation of in-plane seismic retrofit of unreinforced masonry walls by means of vertical steel ties", *Construction and Building Materials*, **52**, pp. 122–129 (2014).

Biographies

Shahrad Ebrahimzadeh received the BSc degree in Civil Engineering from the K. N. Toosi University of Technology, Tehran, Iran in 2013 and MSc degree in Structural Engineering from K. N. Toosi University of Technology, Tehran, Iran in 2017. Currently, he is a PhD candidate in the same field at University of Southern Queensland in Australia. His research interest areas include composite material, numerical analysis by using ABAQUS, optimization, seismic performance of structures, and programming, especially MATLAB.

Kourosh Nasrollahzadeh is an Assistant Professor in Structural Engineering at the Department of Civil Engineering at K.N. Toosi University of Technology in Tehran, Iran. He received the Japan Concrete Institute (JCI) Award for outstanding paper and presentation in two successive years of 2001 and 2002. He was awarded a post-doctoral research fellowship at the University of Tokyo in Japan in 2004–2006. His research interests include seismic retrofitting of structures by FRP, experimental research, and reliability analysis.